THE JOURNAL OF PHYSICAL CHEMISTRY C

Article

pubs.acs.org/JPCC

How Far Can We Probe by SERS?

Gayatri Kumari, Jyothirmayee Kandula, and Chandrabhas Narayana*

Chemistry and Physics of Materials Unit, Jawaharlal Nehru Centre for Advanced Scientific Research, Jakkur P.O., Bangalore 560064, India

Supporting Information

ABSTRACT: Surface-enhanced Raman spectroscopy (SERS) has gained paramount importance in the recent past due to its widespread applications in biodetection, monitoring chemical reactions, small molecule protein interactions, etc. It is believed that SERS is a distance-dependent phenomenon and is effective within 1 nm from the nanoparticle surface. In this work, we have investigated this distance dependence of SERS as a function of nanoparticle size. Earlier attempts have made use of flexible separators, like DNA and chemical molecules, between nanoparticle and analyte to vary the distance. We have used silica coating to vary the distance, without ambiguity, of the analyte from the silver nanoparticle surface. Our results suggest that SERS is observed up to a distance of 1 nm for 20 nm silver nanoparticles juxtaposed to 5 nm in the case of 90 nm silver nanoparticles. This is due to large scattering cross sections and increased radiative damping in the case of the larger nanoparticles. This study gives direct correlation between the size of nanoparticles and distance probed through SERS which would aid in designing nanoparticle system for various applications and analytes in the future.

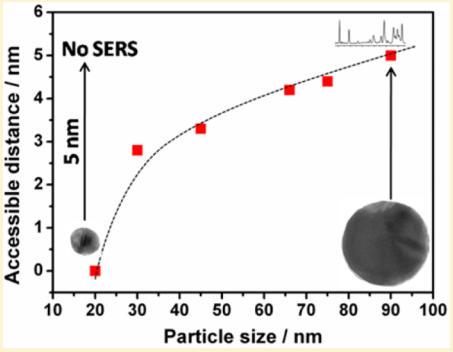

Surface-enhanced Raman spectroscopy (SERS) is the enhancement of Raman signal of molecules present in the vicinity of intense electric field created near a plasmonic nanostructure excited by electromagnetic radiation. The enhancement is due to increased number of photons being scattered by the molecule attributed to higher electric field in the proximity of the nanoparticles (electromagnetic enhancement) and/or due to charge transfer between the molecule and the metal nanoparticles leading to redistribution of molecular energy levels across the Fermi level (chemical enhancement).[1−4] Since its inception, there have been numerous works on developing metal nanostructures[5−8] yielding consistently high SERS enhancement factor, rendering them widely applicable for studying chemical dynamics,[9] single molecule detection,[10−12] single molecule dynamics,[13] DNA detection,[14] investigating conformational changes in protein,[15,16] glucose sensing, and many more.[17] The proximity of the analyte to the nanoparticle surface plays a predominant role in all the applications. It is believed that SERS can be effectively obtained from molecules lying within 1 nm of the nanoparticle surface since the electric field intensity drops by a factor of $1/d^{12}$ with distance.[18] This would substantially affect the SERS signal from larger systems (>1 nm) such as proteins and other macromolecules.

The intense electric field near nanoparticles is due to the excitation of surface plasmons. Free electrons in conduction band of metal nanoparticles can be collectively excited and are confined within the nanoparticle. Once excited, the surface plasmons can decay either radiatively or nonradiatively. Theoretical modeling shows that 20 nm gold nanoparticles are weak scatterers as the surface plasmon damping is mainly governed by energy dissipation via nonradiative processes like electron−electron, electron−phonon, or electron-defect scattering processes while larger gold nanoparticles are strong scatterers as plasmon damping is mainly via the radiative process.[19−21] This means that smaller nanoparticles are weak SERS enhancers in comparison to the larger nanoparticles. It has been shown experimentally that the enhancement factor increases as the nanoparticle size is increased up to a certain limit and thereafter starts decreasing.[22−24] The electric dipole field decays as $1/d^3$, and the plasmonic field decays even more rapidly as $1/d^{12}$, meaning that there will be no SERS enhancement at large distances. The dipolar field is directly proportional to the size of the nanoparticles and the concentration of surface free electron. Hence, to increase the electric field surrounding the nanoparticles, we can increase the size of the nanoparticle and/or increase the charge q by choosing a metal with higher surface free electrons. This implies that the size of nanoparticles plays a vital role in controlling far field enhancement. Recently, nanostructures with 1 nm interior gap have been shown to yield high SERS enhancement factors by Lim et al.[25] Further, modulating interparticle gap in hybrid nanostructures to achieve higher Raman signal have also been reported. Li et al. showed SERS signal decay up to a distance of 20 nm in SHINERS particles,[26,27] while Qin et al. showed highest SERS signal in 30 nm gap between 120 nm nanodisks.[28] Shanthil et al. also showed that the enhancement was higher when the separation between 60 nm silver dimer particles are less than 15 nm.[29]

Received: August 4, 2015
Published: August 5, 2015

DOI: 10.1021/acs.jpcc.5b07556
J. Phys. Chem. C 2015, 119, 20057−20064

While most of the distance-dependent SERS studies are based on single particle size, the result cannot be extrapolated to particles of either smaller or larger sizes. Second, these studies were performed on film or planar substrates. The results may differ from those of colloids in the solution which are primarily employed to study biomolecules wherein charge neutralization and nanoparticle aggregation play a crucial role.

The subject of distant SERS enhancement in colloidal metal nanoparticles of different sizes is still unexplored. In this work we have investigated the role of size of nanoparticles on distance dependence of SERS. Noble metals like copper, silver, and gold are among the best SERS enhancers in the visible region known so far. Among them, silver is the most efficient material as the real part of its dielectric constant is close to −2 in the near-UV while its imaginary part is small, making it the most competent material for surface plasmon excitation as well as SERS.[30] So, we have chosen silver nanoparticles for the present studies. Silver nanoparticles in the size regime of 20−100 nm were synthesized by seed-mediated growth. This approach yields homogeneous nanoparticles which are of utmost importance for this study. For distance-dependent studies, each nanoparticle was coated by thin silica shell of varying thickness. Silica shell prevents direct contact between the analyte molecule and the nanoparticle, thus ensuring enhancement only by electromagnetic mechanism. This is also important when we are using silver nanoparticle for SERS as (a) silver's antibacterial properties could make it difficult for *in vivo* studies of biological samples when used as bare nanoparticles and (b) effect of nanoparticles on the analyte properties, namely, proteins is avoided. The challenge in such a study was preparing controlled SiO_2 coating on nanoparticles, especially coatings of less than 5 nm for bigger nanoparticles. Finally, SERS signal of rhodamine 6G was used to evaluate the distance dependence of the nanoparticles.

Gold nanoparticles of size 12 nm were prepared by the Lee−Meisel method and used as seed for preparation of silver nanoparticles.[31] Silver was reduced by ascorbic acid and capped with sodium citrate. This method yields spherical Au@Ag nanoparticles with a narrow size distribution which is generally difficult to obtain by conventional method of preparation of silver nanoparticles (i.e., reduction of silver salt in the presence of capping agent). To get different sizes of Au@Ag nanoparticles, the ratio of seed nanoparticles to that of silver nitrate was varied. All the silver nanoparticles are citrate capped and hence are negatively charged at pH 7. Figure 1 shows the extinction spectra of silver nanoparticles of size 20 nm (blue), 30 nm (pink), 45 nm (green), 66 nm (purple), 75 nm (sky blue), and 90 nm (red) with the surface plasmon resonances (SPR) occurring at values 392, 401, 412, 433, 439, and 460 nm, respectively. Interestingly, bigger nanoparticles also show higher quadrupole mode around 390 nm, attributable to varying electric field across the nanoparticle.[21] Since the extinction spectrum does not show any plasmon peak corresponding to the gold core, we will be referring Au@Ag nanoparticles as the silver nanoparticles. The systematic increase observed in the SPR position and the line widths with silver nanoparticle size are attributed to the retardation effects and increase in radiation damping, respectively.[19,21] Plasmon damping is chiefly governed by nonradiative processes for smaller nanoparticles whereas for larger particles it is governed by radiative processes making them strong scatterers.[20] Further, it is also known that as the size increases, the fraction of scattering in the extinction increases, making

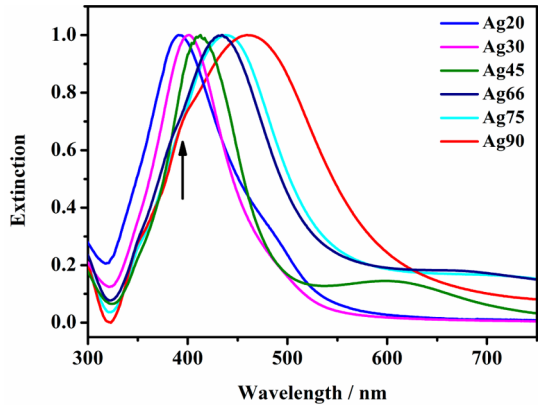

Figure 1. Extinction spectra of silver nanoparticles of size 20 nm (blue), 30 nm (pink), 45 nm (green), 66 nm (purple), 75 nm (sky blue), and 90 nm (red). The arrow shows the appearance of quadrupole mode in larger nanoparticles (Ag75 and Ag90).

larger nanoparticles better scatterers than smaller nanoparticles.[19,32] Additionally, heterogeneity in size, shape, and interaction with surrounding matrix is also known to contribute toward plasmon broadening.[33] TEM image and particle size distribution (Figures S1 and S2, Supporting Information) clearly show the smaller nanoparticles to be homogeneous and larger nanoparticles to be heterogeneous.

Distance-dependent SERS studies necessitate the presence of spacer between the silver surface and the analyte molecules. Many such spacers have been employed in the past, such as double-stranded DNA,[34] thio−methylene spacers,[35] polymer coating (poly(ethylene glycol) or polystyrenesulfonate/poly(diallydimethylammonium hydroxide)),[36,37] silica or alumina coating, etc.[26,29] Each method has its own limitations. Polymer coating yields strong SERS signal of polymer itself while flexibility of DNA chain spacer may yield inaccurate distances. Dielectric coating or silica coating in particular is one of the best ways to maintain distance between silver nanoparticles and analyte molecules in order to monitor the distance dependence in SERS while keeping the environment biocompatible. Our method of thin layer silica coating on smaller nanoparticles (Ag20, Ag30, Ag45, and Ag66) was based on an earlier report by Mulvaney et al.[38] Since the procedure was not suitable for larger nanoparticles, an alternative approach based on the reports of Li et al. and Ung et al. was followed for Ag75 and Ag90 nanoparticles.[26,39] Prior to silica coating, silver nanoparticle surface was functionalized with 3-aminopropyltriethoxysilane or trimethoxysilane. The silica shell was grown using a very low concentration of sodium silicate solution in water. It is known that the silica shell growth is highly dependent on the pH of the solution. At pH 12−14, thick silica shell forms while thin shell formation occurs at pH 9−10.[39] In order to achieve thin silica coating, the pH of sodium silicate solution was reduced to pH 10 by addition of hydrochloric acid or orthophosphoric acid. In addition, silica shell growth is also a function of aging time and temperature. The shell grows slowly at room temperature as the silica condensation reaction rate is low, but the reaction rate increases manyfold as the temperature is raised to 90 °C.[26] The silica shell thickness is increased by aging the solution at 90 °C. To halt the growth process, the reaction is quenched by putting the reaction mixture in an ice bath as reported in previous literature.[26]

Table 1 shows the silver nanoparticle name indicating the silver core size and silica shell thickness. Figures 2−7 show the

DOI: 10.1021/acs.jpcc.5b07556
J. Phys. Chem. C 2015, 119, 20057−20064

Table 1. Nanoparticle Name and the Associated Core Particle Size as Well as the Silica Shell Thickness

nanoparticle name	Au@Ag core particle size (nm)	silica shell thickness (nm)
Ag20@SiO_2_1	20	2.0
Ag30@SiO_2_1	30	2.6
Ag30@SiO_2_2	30	2.8
Ag45@SiO_2_1	45	2.2
Ag45@SiO_2_2	45	3.3
Ag66@SiO_2_1	66	3.2
Ag66@SiO_2_2	66	4
Ag66@SiO_2_3	66	4.2
Ag75@SiO_2_1	75	2.4
Ag75@SiO_2_2	75	2.8
Ag75@SiO_2_3	75	4.4
Ag90@SiO_2_1	90	2.6
Ag90@SiO_2_2	90	3.4
Ag90@SiO_2_3	90	5.0

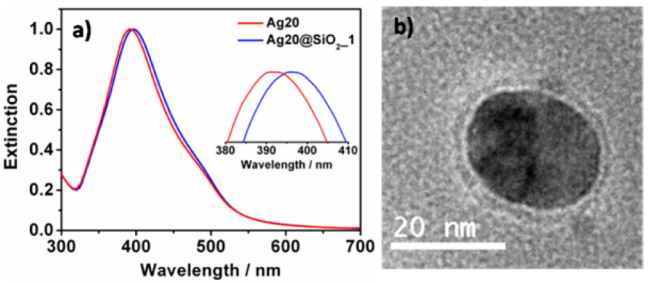

Figure 2. (a) UV−vis spectra of Ag20 and Ag20@SiO_2_1. (b) TEM image of Ag20@SiO_2_1.

extinction spectra of Ag@SiO_2 nanoparticles with 2−5 nm silica coating followed by their TEM images (also see Figures S3−S7, Supporting Information). From the UV−vis spectra, it is observed that the SPR changes only by a few nanometers (∼1 nm) on thin silica coating and is attributed to increase in refractive index of surrounding silica material. It has been shown earlier that the SPR shifts by only 1 nm for thin polymer coating on metal nanoparticles, which conforms with our observation.[40] Thin silica coating on silver nanoparticles is a challenge in itself. Citrate-capped silver nanoparticles are negatively charged, and it is the electrostatic repulsion between the negative charges which prevents the nanoparticle from coalescing. Surface functionalization by APTES/APTMS leads to charge neutralization, resulting in nanoparticle aggregation. To prevent aggregation, a minimum silica coating of 2−4 nm should occur. The synthesis method was optimized to get thin silica coating without aggregation of nanoparticles; nevertheless, we did observe aggregation in the smaller nanoparticles. Further, thin silica coating always yields a range of silica shell thickness. A single particle could also have a variation of ∼1 nm in shell thickness (see Figure 3c). Incidentally, silica coating on the larger nanoparticles was more uniform and had a narrow distribution in comparison to smaller nanoparticles. TEM images in Figures 5, 6, and 7 also show uniform coating on Ag66, Ag75, and Ag90 nanoparticles while that of Ag30@SiO_2 showed coalesced particles although no aggregation peak was seen in the extinction spectra, suggesting that the particles could have aggregated on copper grid used for TEM imaging.

SERS Studies. It is generally believed that SERS primarily occurs within ∼1 nm from the nanoparticle surface. In order to

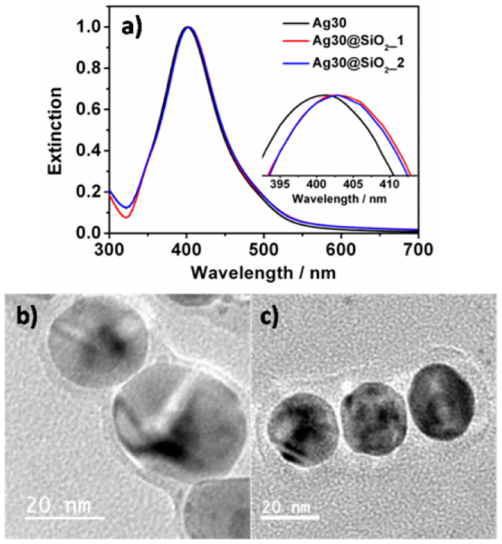

Figure 3. (a) UV−vis spectra of Ag30 and Ag30@SiO_2. TEM image of (b) Ag30@SiO_2_1 and (c) Ag30@SiO_2_2.

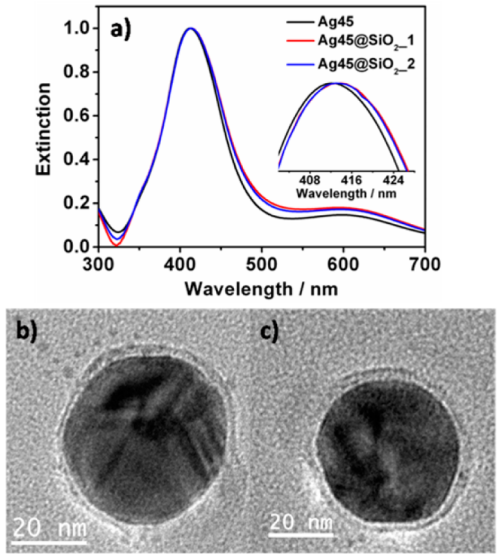

Figure 4. (a) UV−vis spectra of Ag45 and Ag45@SiO_2. TEM image of (b) Ag45@SiO_2_1 and (c) Ag45@SiO_2_2.

prove that the "limit on proximity to the surface" is a function of particle size, SERS of Rhodamine 6G (R6G) was performed on silver nanoparticles of different sizes precoated with variable silica shell thickness. It is well-known that R6G shows surface-enhanced resonant Raman (SERRS) on being excited by a 532 nm laser. Since resonance will not be affecting our conclusion but help in detecting signal at lower concentration, we have used R6G. Figure S8 shows the SERS spectra of 10^{-5} M R6G with 30, 45, 66, 75, and 90 nm silica coated silver nanoparticles. It is observed that there is variation in SERS intensity of R6G. The intensity variation could be due to multiple reasons such as formation of hot spots resulting from aggregation of nanoparticles, plasmon coupling, and formation of new plasmon peaks as a consequence of aggregate formation, etc. Further, the enhancement factor was found to be of the order of 10^3−10^4 for all the nanoparticles; however, their absolute values were different. The SERS signal intensity decayed exponentially for all the Ag nanoparticles and has been plotted in Figure 8. 20

DOI: 10.1021/acs.jpcc.5b07556
J. Phys. Chem. C 2015, 119, 20057−20064

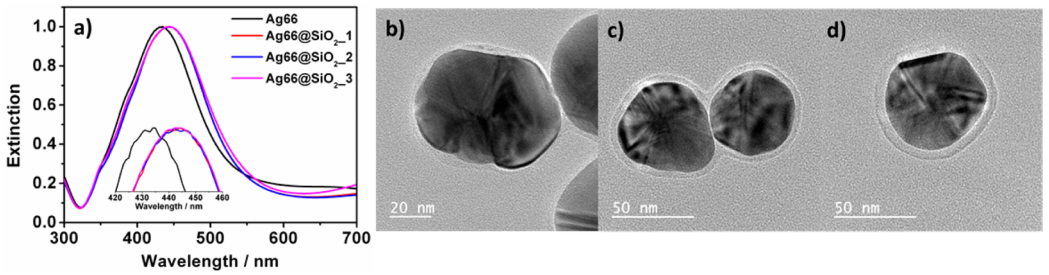

Figure 5. (a) UV−vis spectra of Ag66 and Ag66@SiO_2. TEM image of (b) Ag66@SiO_2_1, (c) Ag66@SiO_2_2, and (d) Ag66@SiO_2_3.

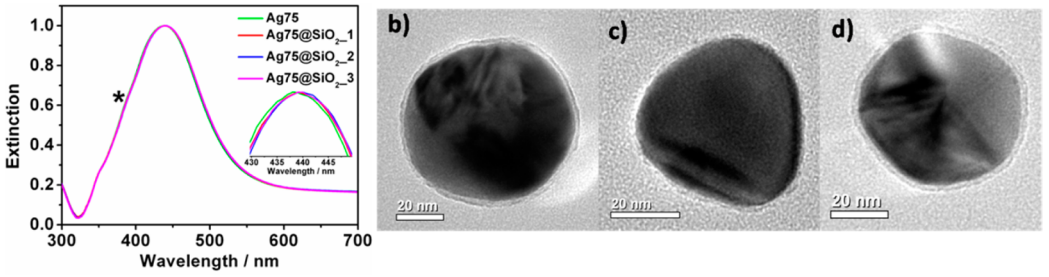

Figure 6. (a) UV−vis spectra of Ag75 and Ag75@SiO_2. TEM image of (b) Ag75@SiO_2_1, (c) Ag75@SiO_2_2, and (d) Ag75@SiO_2_3.

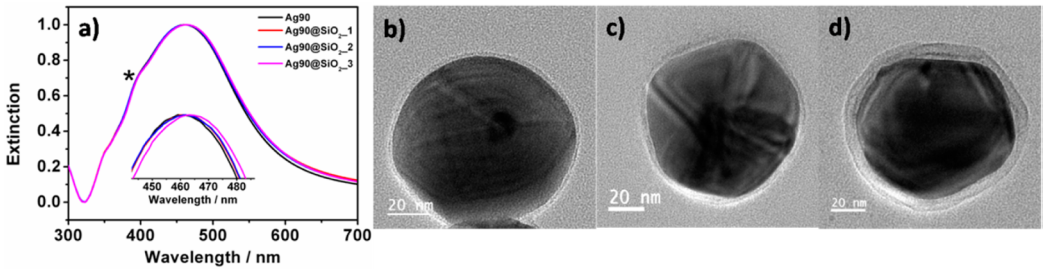

Figure 7. (a) UV−vis spectra of Ag90 and Ag90@SiO_2. TEM image of (b) Ag90@SiO_2_1, (c) Ag90@SiO_2_2, and (d) Ag90@SiO_2_3.

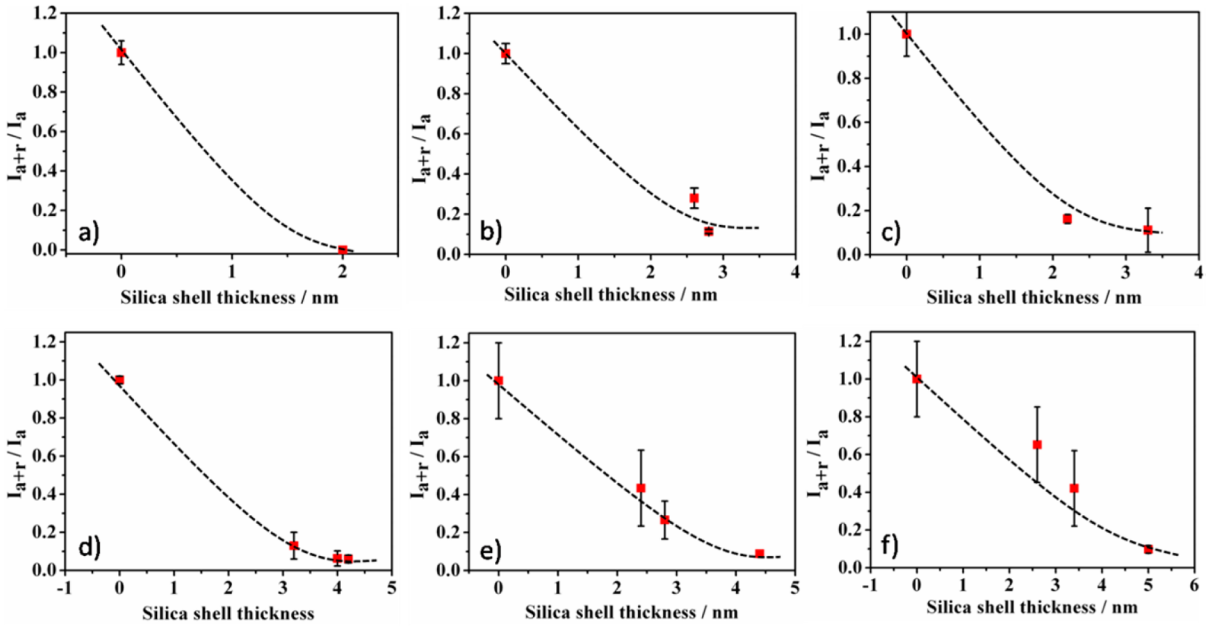

Figure 8. Normalized SERS intensity of 611 cm^{-1} peak of R6G (10^{-5} M) as a function of silica shell thickness for (a) 20, (b) 30, (c) 45, (d) 66, (e) 75, and (f) 90 nm silver nanoparticles. The black dotted line is the guide to the eye.

nm Ag nanoparticles having 2 nm silica shell did not show any SERS signal of R6G while for larger nanoparticles it is observed that the signal intensity decreases as the silica shell thickness increases due to increase in the distance between the analyte

DOI: 10.1021/acs.jpcc.5b07556
J. Phys. Chem. C 2015, 119, 20057−20064

and silver nanoparticle surface. The intensity of C−C−C in-plane ring bending mode at 611 cm^{-1}, a signature peak with sharp feature of R6G, was chosen for determining the SERS intensity as a function of distance.[41,42] Further, the decrease in SERS signal with the increase in distance from the nanoparticle is also indicative of the nonporous nature of silica shell.

For a monolayer of molecule on the nanoparticle surface, SERS intensity decays as $(1 + r/d)^{10}$, where r is the radius of curvature of roughness and d is the distance of molecule from the surface.[43] For 10^{-5} M concentration of R6G chosen in the present work, there is a possibility of multilayer formation on the nanoparticle surface. Hence, the intensity decay does not fit into the above equation. Second, due to the experimental limitation on precisely controlling the silica thickness in the aqueous medium, we could not have many data points to fit into this equation. Empirically, the decay in the SERS intensity is much sharper than what has been reported.[43]

To demonstrate that the "accessible distance", i.e., the distance d from the nanoparticle surface up to which SERS can be observed is a function of nanoparticle size, we have plotted distance d which is nothing but the silica shell thickness (obtained from Figure 8) against silver nanoparticle size in Figure 9. It is noticed that for 30 nm nanoparticle SERS was

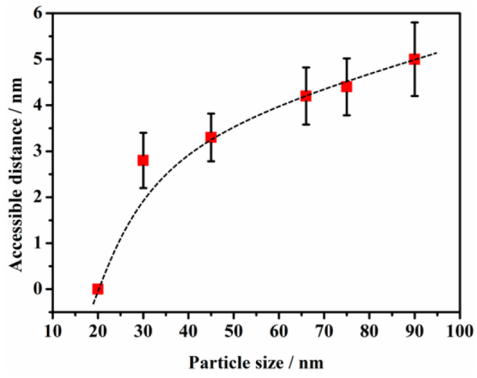

Figure 9. SERS accessible distance as a function Ag nanoparticles size. The black dotted line is the guide to the eye.

observed until a distance of 2.8 nm (which is the thickness of silica shell), while for 45 nm particles, SERS could be recorded as far as 3.2 nm. The farthest point which could be probed increased to 4.4 nm for 75 nm particles. Interestingly, for 90 nm Ag nanoparticles, SERS was observed up to 5 nm from the nanoparticle surface. Here, it must be noted that the accessible distance will not continue to rise with the particle size but would start decreasing after ∼100 nm because nanoparticles larger than 100 nm are not efficient SERS enhancers.[22]

To explain the experimental observation, near field intensity of silica-coated silver nanoparticles was calculated using the finite difference time domain method (FDTD). The electromagnetic wave polarized along x-direction was incident from y-direction onto the nanoparticles as shown in Figure 10. In order to accurately calculate the electric field, smaller mesh size of 0.25 nm was chosen for Ag20 and relatively larger grid size of 0.5 nm was chosen for Ag90 nanoparticles. Perfectly matched layer (PML) boundaries were chosen as they absorb the light entering them. Figure 10 shows the calculated electric field distribution in the vicinity of the nanoparticles on being excited with 532 nm light source. From the FDTD simulations it was observed that the electric field decay is faster for smaller nanoparticles and slows down as the particle size increases. The electric field at a distance of 5 nm from Ag90 nanoparticles was higher, 2.32 V/m in comparison to a value of 1.85 V/m calculated for Ag20 nanoparticles. The field intensity ($|E|^2$) will thus be even larger for larger nanoparticles in comparison to smaller nanoparticles. SERS is proportional to $|E|^4$ wherein not only the incident laser field but the scattered field is also enhanced. Thus, the net enhancement for Ag90 nanoparticles will be very large in comparison the Ag20 nanoparticles. Another feature to be noticed from Figure 10 is the distorted electric field lobe for Ag90 nanoparticles. This is attributed to the presence of varying electric field across larger nanoparticle giving rise to quadrupole mode. The electric field intensity at a distance of 5 nm from all the nanoparticle sizes was calculated by making silica shell thickness of 5 nm. This field is plotted in Supporting Information Figure S9. It can be clearly seen that the field intensity is highest for Ag90 nanoparticles and shows a gradual increase with the size of nanoparticle thus confirming our experimental observation.

In conclusion, we have shown that the accessible distance up to which SERS is observed is strongly dependent on the size of the nanoparticle. This inference was arrived at based on systematic study on Au@Ag@SiO_2 nanoparticles of different Au@Ag core size and silica shell thickness. We could illustrate that the Raman signal can be enhanced even at a distance of 5 nm from the colloidal nanoparticles of 90 nm size, hitherto never demonstrated. Hence, by tuning the Au@Ag nanoparticle size, not only surface modes but other modes of molecules

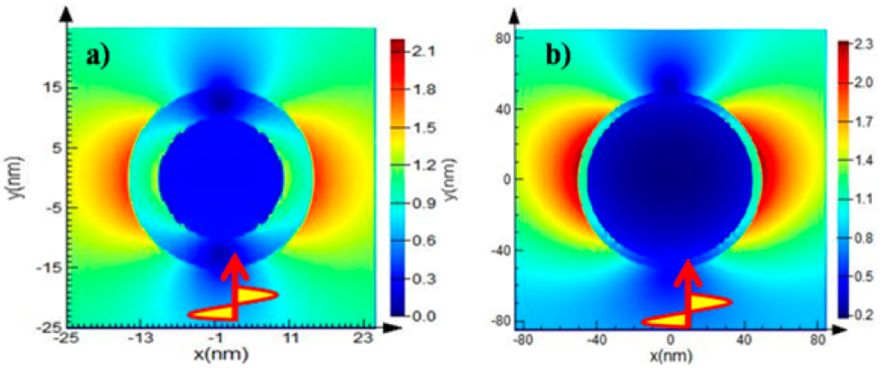

Figure 10. FDTD analysis showing electric field distribution on (a) Ag20 having 5 nm silica shell thickness and (b) Ag90@SiO_2 with 5 nm silica shell thickness. The red arrow shows the direction of incident field along with its polarization direction. The scale runs from −25 to 25 nm in (a) and −85 to 85 nm in (b) on both axes.

DOI: 10.1021/acs.jpcc.5b07556
J. Phys. Chem. C 2015, 119, 20057−20064

which are not in proximity of nanoparticle can also be obtained. Thus, the statement that SERS occurs for molecule at 1 nm from the nanoparticle surface is true only for smaller and isolated nanoparticles bearing a monolayer of molecule. Since most biomolecular studies are conducted in aqueous medium where it is difficult to have control on monolayer formation and nanoparticle aggregation, we need to critically choose the size of nanoparticle which can give the best information. This result will be helpful in selecting the nanoparticle size depending on the size of analyte system. For instance, SERS studies of macromolecules, polymers, or proteins using larger nanoparticles (90 nm) can give better information in comparison to that obtained using smaller nanoparticles, as the vibrational modes buried deep inside proteins will also be electromagnetically enhanced and may appear in SERS spectrum except when it is forbidden due to the selection rules.

EXPERIMENTAL METHODS

Chemicals. $HAuCl_4$ (Spectrochem, India), sodium citrate (Sigma-Aldrich), silver nitrate (Sigma-Aldrich), ascorbic acid (Rankem), 3-aminopropyltriethosysilane (APTES, Merck), 3-aminopropyltrimethoxysilane (APTMS, Sigma-Aldrich), ethanol (Commercial Alcohols, AR), sodium silicate (27% in water, Sigma-Aldrich), sodium hydroxide (Merck), orthophosphoric acid (S D Fine-Chem Limited), and hydrochloric acid (S D Fine-Chem Limited). For all the synthesis Milli-Q water was used, and the glasswares were thoroughly washed before use.

Active Silica.[38] 72 μL of 27% sodium silicate was added to 3.528 mL of water in a beaker. In another beaker, 0.6 g of NaOH was added to 5 mL of water. The two solutions were mixed to form active silica.

Sodium Silicate Solution (for Ag75).[26] 200 μL of sodium silicate solution was added to 2 mL of water. To this, 6 mL of 0.01 M HCl solution was added with fast stirring. Further, 1.8 mL of water was added to make 0.54% solution of sodium silicate with a pH of 10. The solution was freshly prepared before use.

Sodium Silicate Solution (for Ag90).[26] 30 μL of orthophosphoric acid was added to 20 mL of water in a beaker to make 22 mM solution. In another beaker 500 μL of sodium silicate was added to 5 mL of water. 15 mL of 22 mM orthophosphoric acid solution was added to sodium silicate solution. The solution was freshly prepared before use.

Synthesis of Gold Seed by the Lee–Meisel Method. Gold nanoparticles of size 12 nm were prepared via the Lee–Meisel method.[31] Briefly, 48 mg of $HAuCl_4$ was added to 100 mL of water and brought to boiling. 10 mL of 1% sodium citrate was added, and the solution was further boiled for 1 h.

Growth of Silver over Gold Seed. To obtain silver nanoparticles of uniform size, seed mediated growth approach reported for by Uzayisenga et al. was adopted.[44] The synthesis protocol was further optimized to obtain even bigger silver nanoparticles by varying the ratio of Au seed to silver salt. Breifly, gold nanoparticle was diluted with Milli-Q water followed by addition of sodium citrate (1% solution in water) and ascorbic acid (10 mM) as given in the Supporting Information Table S1. The mixture was stirred for 5 min, after which silver nitrate (10 mM in water) solution was added dropwise and aged at 100 °C for 2 h.

Thin Silica Coating. The silica coating procedures reported in the literature can be categorized into two categories. The first one is based on Stober's method which describes the coating using tetraethyl orthosilicate (TEOS) in ethanol or propanol–water mixture. The second synthesis was developed by Liz-Marzàn and Paul Mulvaney using sodium silicate solution.[38,39] Apparently, Stober's method can be best applied for thick silica coating of tens of nanometers of silica, while the second method is suited for thin layer silica coating of few nanometers. Since our interests lay in thin layer silica coating, we followed the approach given by Liz-Marzàn and Paul Mulvaney.[38,39] We have used a modified protocol to coat thin layer silica on Au@Ag based on earlier reports.[26,38] Slightly different procedures were used for different size of Au@Ag nanoparticles as described below.

Ag20@SiO_2. 5 mL of Ag20 was added to 5 mL water and stirred. 20 μL of 2 mM APTES (in ethanol) was added and stirred for 15 min, followed by addition of 20 μL of active silica (see above for preparation of active silica). The solution was left undisturbed for 2 h, after which they were centrifuged and redispersed in Milli-Q water. In order to get different silica coating thickness, the amount of active silica and the time for silica condensation were varied.

Ag30@SiO_2. 5 mL of Ag30 was added to 5 mL of water and stirred. 10 μL of 2 mM APTES (in ethanol) was added and stirred for 15 min. Then 10 μL of active silica was added and the solution was left undisturbed for 2 h. Further, the nanoparticles were centrifuged and redispersed in Milli-Q water. Similar procedures were followed for Ag45 and Ag66 nanoparticles. See Tables S2 and S3 in the Supporting Information for experimental details.

Ag75@SiO_2 and Ag90@SiO_2. Silver nanoparticles were functionalized with 1 mM APTES solution. Then, 0.54% sodium silicate solution was added and heated at 90 °C. After heating for specified time given in Tables S4 and S5 of the Supporting Information, the reaction was quenched by transferring the solution in a 1.5 mL centrifuge tube and putting in an ice bath. After 30 min, the solutions were centrifuged, washed with water once, and redispersed in Milli-Q water. The silica-coated nanoparticles were stored in fridge at 4 °C. For further experimental details, refer to the procedure summarized in Tables S3 and S4 of the Supporting Information.

Characterization. The nanoparticles were characterized by UV–vis spectroscopy and transmission electron microscopy. UV–vis spectra of dilute solutions of nanoparticle were recorded in a 1 cm quartz cell using a PerkinElmer Lambda 900 spectrometer. For TEM measurements, JEOL 3010 with an operating voltage of 300 keV was used. TEM samples were prepared by drop-coating nanoparticle solution on a Formvar-film-covered carbon-coated copper grid. Particles size distribution was calculated from TEM images through digital micrograph imaging software.

Raman and SERS measurements were conducted on a custom-built Raman microscope equipped with 532 nm wavelength laser provided by solid state frequency-doubled Nd:YAG laser, described elsewhere.[45] The accumulation time for each spectrum was 10 s. For SERS studies, 5 μL of nanoparticles was mixed with 5 μL of 10^{-5} M R6G solution in water. 1 μL of the mixture was drop-casted on a cleaned glass slide and dried in a desiccator.

ASSOCIATED CONTENT

Supporting Information

The Supporting Information is available free of charge on the ACS Publications website at DOI: 10.1021/acs.jpcc.5b07556.

DOI: 10.1021/acs.jpcc.5b07556
J. Phys. Chem. C 2015, 119, 20057–20064

Synthesis details, tables, particle size histograms, TEM images, SERS intensity decay plot and enhancement factor calculation, FDTD simulation details (PDF)

AUTHOR INFORMATION

Corresponding Author

*E-mail: cbhas@jncasr.ac.in (C.N.).

Notes

The authors declare no competing financial interest.

ACKNOWLEDGMENTS

The authors acknowledge JNCASR for providing the financial support. G.K. is thankful to Dr. Usha Tumkurkar for TEM measurements.

REFERENCES

(1) Moskovits, M. Surface-Enhanced Spectroscopy. *Rev. Mod. Phys.* **1985**, *57*, 783−826.

(2) Stiles, P. L.; Dieringer, J. A.; Shah, N. C.; Van Duyne, R. P. Surface-Enhanced Raman Spectroscopy. *Annu. Rev. Anal. Chem.* **2008**, *1*, 601−626.

(3) Creighton, J. A. Surface Raman Electromagnetic Enhancement Factors for Molecules at the Surface of Small Isolated Metal Spheres: The Determination of Adsorbate Orientation from SERS Relative Intensities. *Surf. Sci.* **1983**, *124*, 209−219.

(4) Valley, N.; Greeneltch, N.; Van Duyne, R. P.; Schatz, G. C. A Look at the Origin and Magnitude of the Chemical Contribution to the Enhancement Mechanism of Surface-Enhanced Raman Spectroscopy (SERS): Theory and Experiment. *J. Phys. Chem. Lett.* **2013**, *4*, 2599−2604.

(5) Vigderman, L.; Zubarev, E. R. Starfruit-Shaped Gold Nanorods and Nanowires: Synthesis and SERS Characterization. *Langmuir* **2012**, *28*, 9034−9040.

(6) Kumari, G.; Narayana, C. New Nano Architecture for SERS Applications. *J. Phys. Chem. Lett.* **2012**, *3*, 1130−1135.

(7) Cho, W. J.; Kim, Y.; Kim, J. K. Ultrahigh-Density Array of Silver Nanoclusters for SERS Substrate with High Sensitivity and Excellent Reproducibility. *ACS Nano* **2012**, *6*, 249−255.

(8) Lee, J.−H.; Nam, J.−M.; Jeon, K.-S.; Lim, D.-K.; Kim, H.; Kwon, S.; Lee, H.; Suh, Y. D. Tuning and Maximizing the Single-Molecule Surface-Enhanced Raman Scattering from DNA-Tethered Nanodumbbells. *ACS Nano* **2012**, *6*, 9574−9584.

(9) Xie, W.; Walkenfort, B.; Schlücker, S. Label-Free SERS Monitoring of Chemical Reactions Catalyzed by Small Gold Nanoparticles Using 3D Plasmonic Superstructures. *J. Am. Chem. Soc.* **2013**, *135*, 1657−1660.

(10) Le Ru, E. C.; Etchegoin, P. G. Single-Molecule Surface-Enhanced Raman Spectroscopy. *Annu. Rev. Phys. Chem.* **2012**, *63*, 65−87.

(11) Zhang, R.; Zhang, Y.; Dong, Z. C.; Jiang, S.; Zhang, C.; Chen, L. G.; Zhang, L.; Liao, Y.; Aizpurua, J.; Luo, Y.; Yang, J. L.; Hou, J. G. Chemical Mapping of a Single Molecule by Plasmon-Enhanced Raman Scattering. *Nature* **2013**, *498*, 82−86.

(12) Qian, X.-M.; Nie, S. M. Single-Molecule and Single-Nanoparticle SERS: From Fundamental Mechanisms to Biomedical Applications. *Chem. Soc. Rev.* **2008**, *37*, 912−920.

(13) Konishi, T.; Kiguchi, M.; Takase, M.; Nagasawa, F.; Nabika, H.; Ikeda, K.; Uosaki, K.; Ueno, K.; Misawa, H.; Murakoshi, K. Single Molecule Dynamics at a Mechanically Controllable Break Junction in Solution at Room Temperature. *J. Am. Chem. Soc.* **2013**, *135*, 1009−1014.

(14) Kneipp, K.; Kneipp, H.; Kartha, V. B.; Manoharan, R.; Deinum, G.; Itzkan, I.; Dasari, R. R.; Feld, M. S. Detection and Identification of a Single DNA Base Molecule Using Surface-Enhanced Raman Scattering (SERS). *Phys. Rev. E: Stat. Phys., Plasmas, Fluids, Relat. Interdiscip. Top.* **1998**, *57*, R6281−R6284.

(15) Karthigeyan, D.; Siddhanta, S.; Kishore, A. H.; Perumal, S. S. R. R.; Ågren, H.; Sudevan, S.; Bhat, A. V.; Balasubramanyam, K.; Subbegowda, R. K.; Kundu, T. K.; Narayana, C. SERS and MD Simulation Studies of a Kinase Inhibitor Demonstrate the Emergence of a Potential Drug Discovery Tool. *Proc. Natl. Acad. Sci. U. S. A.* **2014**, *111*, 10416−10421.

(16) Kundu, P. P.; Bhowmick, T.; Swapna, G.; Pavan Kumar, G. V.; Nagaraja, V.; Narayana, C. Allosteric Transition Induced by Mg^{2+} Ion in a Transactivator monitored by SERS. *J. Phys. Chem. B* **2014**, *118*, 5322−5330.

(17) Schlücker, S. Surface-Enhanced Raman Spectroscopy: Concepts and Chemical Applications. *Angew. Chem., Int. Ed.* **2014**, *53*, 4756−4795.

(18) Campion, A.; Kambhampati, P. Surface-Enhanced Raman Scattering. *Chem. Soc. Rev.* **1998**, *27*, 241−250.

(19) Kreibig, U.; Vollmer, M. *Optical Properties of Metal Clusters*; Springer: Berlin, 1998.

(20) Kolwas, K.; Derkachova, A. Plasmonic Abilities of Gold and Silver Spherical Nanoantennas in Terms of Size Dependent Multipolar Resonance Frequencies and Plasmon Damping Rates. *Opto-Electron. Rev.* **2010**, *18*, 429−437.

(21) Sönnichsen, C.; Franzl, T.; Wilk, T.; von Plessen, G.; Feldmann, J. Plasmon Resonances in Large Noble-Metal Clusters. *New J. Phys.* **2002**, *4*, 93.1−93.8.

(22) Stamplecoskie, K. G.; Scaiano, J. C. Optimal Size of Silver Nanoparticles for Surface-Enhanced Raman Spectroscopy. *J. Phys. Chem. C* **2011**, *115*, 1403−1409.

(23) Lin, W.-C.; Liao, L.-S.; Chen, Y.-H.; Chang, H.-C.; Tsai, D. P.; Chiang, H.-P. Size Dependence of Nanoparticle-SERS Enhancement from Silver Film over Nanosphere (AgFON) Substrate. *Plasmonics* **2011**, *6*, 201−206.

(24) Fang, P.-P.; Li, J.-F.; Yang, Z.-L.; Li, L.-M.; Ren, B.; Tian, Z.-Q. Optimization of SERS Activities of Gold Nanoparticles and Gold-Core−Palladium-Shell Nanoparticles by Controlling Size and Shell Thickness. *J. Raman Spectrosc.* **2008**, *39*, 1679−1687.

(25) Lim, D.-K.; Jeon, K.-S.; Hwang, J.-H.; Kim, H.; Kwon, S.; Suh, Y. D.; Nam, J.-M. Highly Uniform and Reproducible Surface-Enhanced Raman Scattering from DNA-Tailorable Nanoparticles with 1-nm Interior Gap. *Nat. Nanotechnol.* **2011**, *6*, 452−460.

(26) Li, J. F.; Tian, X. D.; Li, S. B.; Anema, J. R.; Yang, Z. L.; Ding, Y.; Wu, Y. F.; Zeng, Y. M.; Chen, Q. Z.; Ren, B.; Wang, Z. L.; Tian, Z. Q. Surface Analysis Using Shell-Isolated Nanoparticle Enhanced Raman Spectroscopy. *Nat. Protoc.* **2013**, *8*, 52−65.

(27) Li, J. F.; Huang, Y. F.; Ding, Y.; Yang, Z. L.; Li, S. B.; Zhou, X. S.; Fan, F. R.; Zhang, W.; Zhou, Z. Y.; Wu, D. Y.; Ren, B.; Wang, Z. L.; Tian, Z. Q. Shell-Isolated Nanoparticle-Enhanced Raman Spectroscopy. *Nature* **2010**, *464*, 392−395.

(28) Qin, L.; Zou, S.; Xue, C.; Atkinson, A.; Schatz, G. C.; Mirkin, C. A. Designing, Fabricating, and Imaging Raman Hot Spots. *Proc. Natl. Acad. Sci. U. S. A.* **2006**, *103*, 13300−13303.

(29) Shanthil, M.; Thomas, R.; Swathi, R. S.; Thomas, K. G. Ag@SiO_2 Core−Shell Nanostructures: Distance-Dependent Plasmon Coupling and SERS Investigation. *J. Phys. Chem. Lett.* **2012**, *3*, 1459−1464.

(30) Johnson, P. B.; Christy, R. W. Optical constants of the noble metals. *Phys. Rev. B* **1972**, *6*, 4370−4379.

(31) Lee, P. C.; Meisel, D. Adsorption and Surface-Enhanced Raman of Dyes on Silver and Gold Sols. *J. Phys. Chem.* **1982**, *86*, 3391−3395.

(32) Jain, P. K.; Lee, K. S.; El-Sayed, I. H.; El-Sayed, M. A. Calculated Absorption and Scattering Properties of Gold Nanoparticles of Different Size, Shape, and Composition: Applications in Biological Imaging and Biomedicine. *J. Phys. Chem. B* **2006**, *110*, 7238−7248.

(33) Hovel, H.; Fritz, S.; Hilger, A.; Kreibig, U.; Vollmer, M. Width of Cluster Plasmon Resonances: Bulk Dielectric Functions and Chemical Interface Damping. *Phys. Rev. B: Condens. Matter Mater. Phys.* **1993**, *48*, 18178−18188.

(34) Singh, A. K.; Khan, S. A.; Fan, Z.; Demeritte, T.; Senapati, D.; Kanchanapally, R.; Ray, P. C. Development of a Long-Range Surface-

DOI: 10.1021/acs.jpcc.5b07556
J. Phys. Chem. C 2015, 119, 20057−20064

Enhanced Raman Spectroscopy Ruler. *J. Am. Chem. Soc.* **2012**, *134*, 8662−8669.
(35) Kennedy, B. J.; Spaeth, S.; Dickey, M.; Carron, K. T. Determination of the Distance Dependence and Experimental Effects for Modified SERS Substrates Based on Self-Assembled Monolayers Formed Using Alkanethiols. *J. Phys. Chem. B* **1999**, *103*, 3640−3646.
(36) Radziuk, D.; Moehwald, H. Highly Effective Hot Spots for SERS Signatures of Live Fibroblasts. *Nanoscale* **2014**, *6*, 6115−6126.
(37) Gittins, D. I.; Caruso, F. Tailoring the Polyelectrolyte Coating of Metal Nanoparticles. *J. Phys. Chem. B* **2001**, *105*, 6846−6852.
(38) Mulvaney, S. P.; Musick, M. D.; Keating, C. D.; Natan, M. J. Glass-Coated, Analyte-Tagged Nanoparticles: A New Tagging System Based on Detection with Surface-Enhanced Raman Scattering. *Langmuir* **2003**, *19*, 4784−4790.
(39) Ung, T.; Liz-Marzán, L. M.; Mulvaney, P. Controlled Method for Silica Coating of Silver Colloids. Influence of Coating on the Rate of Chemical Reactions. *Langmuir* **1998**, *14*, 3740−3748.
(40) Kobayashi, Y.; Katakami, H.; Mine, E.; Nagao, D.; Konno, M.; Liz-Marzán, L. M. Silica Coating of Silver Nanoparticles Using a Modified Stöber Method. *J. Colloid Interface Sci.* **2005**, *283*, 392−396.
(41) Hildebrandt, P.; Stockburger, M. Surface-Enhanced Resonance Raman Spectroscopy of Rhodamine 6G Adsorbed on Colloidal Silver. *J. Phys. Chem.* **1984**, *88*, 5935−5944.
(42) Kudelski, A. Raman Studies of Rhodamine 6G and Crystal Violet Sub-Monolayers on Electrochemically Roughened Silver Substrates: Do Dye Molecules Adsorb Preferentially on Highly SERS-Active Sites? *Chem. Phys. Lett.* **2005**, *414*, 271−275.
(43) Dieringer, J. A.; McFarland, A. D.; Shah, N. C.; Stuart, D. A.; Whitney, A. V.; Yonzon, C. R.; Young, M. A.; Zhang, X.; Van Duyne, R. P. Surface Enhanced Raman Spectroscopy: New Materials, Concepts, Characterization Tools, and Applications. *Faraday Discuss.* **2006**, *132*, 9−26.
(44) Uzayisenga, V.; Lin, X.-D.; Li, L.-M.; Anema, J. R.; Yang, Z.-L.; Huang, Y.-F.; Lin, H.-X.; Li, S.-B.; Li, J.-F.; Tian, X.-Q. Synthesis, Characterization, and 3D-FDTD Simulation of Ag@SiO_2 Nanoparticles for Shell-Isolated Nanoparticle-Enhanced Raman Spectroscopy. *Langmuir* **2012**, *28*, 9140−9146.
(45) Kumar, G. V. P.; Narayana, C. Adapting a Fluorescence Microscope to Perform Surface Enhanced Raman Spectroscopy. *Curr. Sci.* **2007**, *93*, 778−781.

DOI: 10.1021/acs.jpcc.5b07556
J. Phys. Chem. C 2015, 119, 20057−20064